33rd Annual International Conference of the IEEE EMBS
Boston, Massachusetts USA, August 30 - September 3, 2011

Contour Detection of Atherosclerotic Plaques in IVUS Images Using Ellipse Template Matching and Particle Swarm Optimization

Qi Zhang, *Member, IEEE*, Yuanyuan Wang, *Senior Member, IEEE*, Jianying Ma, and Jun Shi

***Abstract*—It is valuable for diagnosis of atherosclerosis to detect lumen and media-adventitia contours in intravascular ultrasound (IVUS) images of atherosclerotic plaques. In this paper, a method for contour detection of plaques is proposed utilizing the prior knowledge of elliptic geometry of plaques. Contours are initialized as ellipses by using ellipse template matching, where a matching function is maximized by particle swarm optimization. Then the contours are refined by boundary vector field snakes. The method was evaluated via 88 *in vivo* images from 21 patients. It outperformed a state-of-the-art method by 3.8 pixels and 4.8% in terms of the mean distance error and relative mean distance error, respectively.**

I. Introduction

ATHEROSCLEROSIS, a vascular disease, is a major cause of mortality in industrialized countries. Intravascular ultrasound (IVUS) is a real-time, high resolution, and invasive imaging modality, which provides a valuable technique for diagnosis of atherosclerosis. Contour detection of atherosclerotic plaques is a crucial step for quantitative assessment of atherosclerosis. It consists of detection of two contours, including lumen and media-adventitia contours. The contour detection is traditionally achieved by manually tracing the two contours by physicians. However, it is tedious, time-consuming, and subject to physicians' experience.

To overcome the drawbacks of manual tracing, several research groups have investigated automated methods. There are mainly two categories of methods according to the information they use. The first is driven by region information [1-2]. It models gray level distribution of various regions in images and discriminates the regions to delineate borders between them. But the accuracy of the modeling is usually degenerated due to artifacts, as well as complex components in plaques, such as calcifications and lipid pools. The second category of methods is those based on edge information [3-4]. It captures and connects edges in images, which are represented by large gradient, variance, or other characteristics. This category of methods generally takes advantage of snakes, also known as active contour models, to deform an initial contour and converge it to a final one by using the edge information [4]. However, speckle noise contaminates IVUS images and results in low signal-to-noise ratios [2], leading to many spurious edges in the images and limiting the precision of contour detection.

In order to improve the accuracy of contour detection, other types of information besides region and edge information need to be explored and utilized. Liu *et al.* [5] noticed that the geometry of objects (thermal lesions) at elastographic images are close to circles, so they used the circle template matching to detect contours of the objects with the help of the prior knowledge of geometry. Inspired by their work, we notice that there is also prior knowledge of object geometry in IVUS images. Due to blood pressure and vessel wall elasticity, the geometry of the lumen and media-adventitia contours tends to be ellipse [6-7]. Therefore, in this paper, the prior knowledge of elliptic geometry is incorporated in the contour detection to initialize snakes, which are then driven by the edge information and refined to yield the final contours.

II. Methods

We propose a method using ellipse template matching and particle swarm optimization (PSO) to automatically initialize the lumen and media-adventitia contours. Contour refinement is then conducted at the boundary vector field (BVF) to evolve the initial contours until they converge to final ones.

A. Extraction of Regions of Interest

To automate procedures of contour detection and reduce computing time, regions of interest (ROIs) are automatically extracted from IVUS images. We first crop each image to a 10×10 mm^2 sub-image whose center is the catheter's center. The sub-image serves as the ROI for media-adventitia contour detection. After the media-adventitia contour is detected, a new ROI, which is 15% larger than the area inside the media-adventitia contour, is extracted for lumen contour detection.

B. Ellipse Template Matching

The ellipse function is defined with five parameters:

$$F(x_c, y_c, r_a, r_b, \theta) = \left[(x-x_c)\cos\theta + (y-y_c)\sin\theta\right]^2 / r_a^2 + \left[(x-x_c)\sin\theta - (y-y_c)\cos\theta\right]^2 / r_b^2, \quad (1)$$

where x_c and y_c are the coordinates of the ellipse center, r_a and r_b are half the lengths of the major and minor axes of the ellipse respectively, and θ is the orientation of the ellipse.

We then design an ellipse template function $T(x, y)$ as follows:

Manuscript received March 25, 2011. This work was supported in part by the Leading Academic Discipline Project of Shanghai Educational Committee (J50104) and Innovation Fund of Shanghai University (10010710007).

Qi Zhang and Jun Shi are with the School of Communication and Information Engineering, Shanghai University, 200072, China (phone: 86-21-56331787; fax: 86-21-56333213; e-mail: zhangq@shu.edu.cn).

Yuanyuan Wang and Jianying Ma are with Fudan University, Shanghai, 200433, China. (e-mail: yywang@fudan.edu.cn; mjy7307@163.com).

$$T_{x_c,y_c,r_a,r_b,\theta}(x,y)=\begin{cases}-1, \text{if } F(x_c,y_c,r_a,r_b,\theta)\le 1\\ 1, \text{if } 1<F(x_c,y_c,r_a,r_b,\theta)\le 2\\ T_{bg}, \text{elsewhere}\end{cases}. \quad (2)$$

The template is comprised of three regions, including the inner ellipse, the region between inner and outer ellipses and the region outside the outer ellipse. The intensities at the three regions are -1, 1, and T_{bg}, respectively, where $T_{bg} \in [-1, 1]$.

We define a matching function as the sum of the products of the template $T(x, y)$ and the image being analyzed $I(x, y)$:

$$M(x_c,y_c,r_a,r_b,\theta)=\sum_{x,y}\left[T_{x_c,y_c,r_a,r_b,\theta}(x,y)\cdot I(x,y)\right]. \quad (3)$$

An elliptic object can be found when (3) is maximized:

$$(x_c^*,y_c^*,r_a^*,r_b^*,\theta^*)=\underset{x_c,y_c,r_a,r_b,\theta}{\text{argmax}}\, M(x_c,y_c,r_a,r_b,\theta). \quad (4)$$

Here, x_c*, y_c*, r_a*, r_b*, and θ* denote the parameters of the ellipse which optimally approximates to the object.

It is indicated from (2) that the region between inner and outer ellipses is positive for the summing in (3), whereas the inner ellipse is negative. Thus an elliptic object with a low gray level, in a background with a high gray level, can be detected by the ellipse template matching. Because there are two contours being detected, the "object" and "background" have different meanings for different tasks. For the lumen contour detection, the object should be small, only containing lumen, and the background should include plaque and adventitia. For the media-adventitia contour detection, the object should be large, consisting of lumen and plaque, and the background should only contain adventitia. As an example, simplified structures in an IVUS image is seen in Fig. 1a, where the regions corresponding to lumen, plaque and adventitia are indicated. Fig. 1b and Fig. 1c illustrate different meanings of objects and backgrounds for detection of lumen and media-adventitia contours, respectively, where the objects are superimposed with white dots.

The parameter T_{bg} in (2), i.e., the intensity outside the outer ellipse in the template, controls the template matching to search for different sizes of ellipses in the image, thus it can be adjusted to detect the two contours. When T_{bg} is large (e.g., let it take the extreme value, 1), two regions including the regions outside the outer ellipse and between two ellipses, are positive for the summing in (3), whereas only the inner ellipse affects the summing negatively. Therefore the template tends to shrink when maximizing (3), implying it is suitable for lumen contour detection. When T_{bg} is small (e.g., let it take the extreme value, -1), two regions consisting of the inner ellipse and the region outside the outer ellipse affect negatively on the summing, and only the region between two ellipses is positive. Thus the template inclines to expansion to maximize (3), implying it is suitable for media-adventitia contour detection. In this paper, we empirically set T_{bg} to 0.3 and -0.7 for lumen and media-adventitia contour detection, respectively. As an example, Fig. 1d and Fig. 1e show two ellipse templates matched for lumen and media-adventitia contours, respectively.

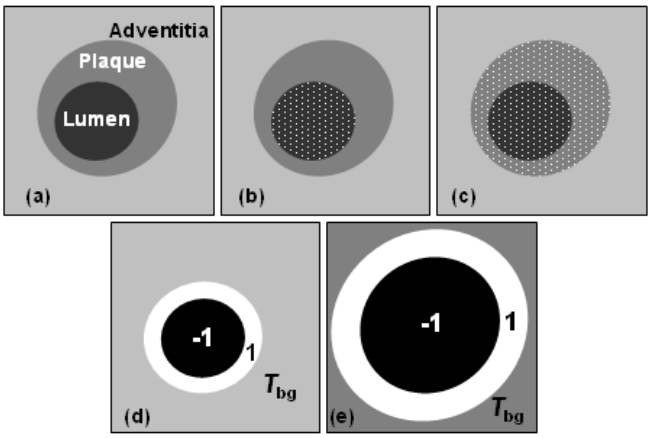

Fig. 1. Ellipse template matching. (a) Simplified structures in an IVUS image; (b, c) the object (dotted area) and background when detecting the lumen contour and the media-adventitia contour, respectively; and (d, e) ellipse templates which are matched for (b) and (c), respectively.

C. Particle Swarm Optimization

The maximization problem shown in (4) can be solved by exhaustive search, which is very time consuming. Thus it is necessary to solve it by optimization algorithms. PSO is a population-based evolutionary computation technique exploiting cooperative and social aspects of the biological phenomena [8-9]. PSO iteratively moves individuals (i.e., particles) in a population (i.e., a swarm) in the search space and eventually finds the optimal solution. The iteration equations of the conventional PSO are given by [8-9]:

$$\boldsymbol{v}_i(k+1)=\varphi(k)\boldsymbol{v}_i(k)+\alpha_1\gamma_{1i}[\boldsymbol{p}_i-\boldsymbol{x}_i(k)]+\alpha_2\gamma_{2i}[\boldsymbol{G}-\boldsymbol{x}_i(k)], \quad (5)$$

$$\boldsymbol{x}_i(k+1)=\boldsymbol{x}_i(k)+\boldsymbol{v}_i(k+1), \quad (6)$$

where $\boldsymbol{x}_i(k) = [x_{c,i}(k), y_{c,i}(k), r_{a,i}(k), r_{b,i}(k), \theta_i(k)]$ denotes the position of ith particle at the kth iteration, $\boldsymbol{v}_i$ is the velocity of the particle, $\boldsymbol{p}_i$ and $\boldsymbol{G}$ are the personal and global best positions, respectively. $\varphi(k)$ is an inertial function, α_1 and α_2 are acceleration constants, and γ_{1i} and γ_{2i} are random numbers.

In this paper, we use a variation of PSO which integrates PSO with genetic algorithms [8-9]. After particle positions are updated in each iteration, particles are selected, in pairs, for crossover. For each pair, two child particles are generated by a crossover rule and replace the parents, and their positions and velocities are given by:

$$\boldsymbol{x}_i'=p\boldsymbol{x}_i+(1-p)\boldsymbol{x}_j,\ \boldsymbol{x}_j'=p\boldsymbol{x}_j+(1-p)\boldsymbol{x}_i, \quad (7)$$

$$\boldsymbol{v}_i'=|\boldsymbol{v}_i|\boldsymbol{V},\boldsymbol{v}_j'=|\boldsymbol{v}_j|\boldsymbol{V}, \text{where } \boldsymbol{V}=(\boldsymbol{v}_i+\boldsymbol{v}_j)/|\boldsymbol{v}_i+\boldsymbol{v}_j|, \quad (8)$$

where p is a random probability.

The hybrid PSO enhances searching the space between particles. Via crossover, the searching may skip off from the local maxima and approach the global maxima. However, blindly using hybrid PSO is not appropriate in the ellipse template matching. It needs to be reconsidered. In the early stage of searching, it is helpful to use the hybrid PSO to expand exploration of the global maxima. In the late stage, the searching algorithm needs to precisely locate the maxima, but the crossover might delay or even disturb the progress. Therefore, we propose a new rule to meet the requirements of both global exploration and precise localization. When the

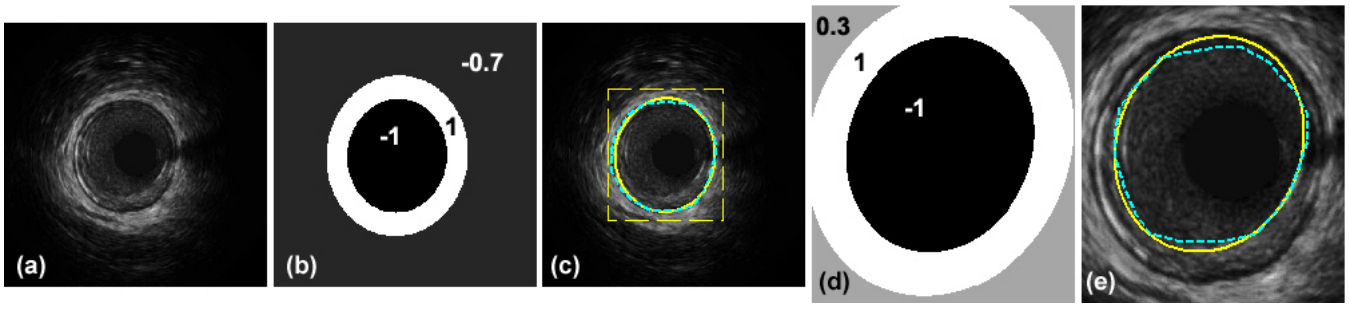

Fig. 2. Results of contour initialization. (a) An ROI for media-adventitia contour detection; (b) the ellipse template matched for the media-adventitia contour; (c) the detected (yellow solid line) and manually traced (cyan dashed line) media-adventitia contours, and the new ROI for lumen contour detection (yellow dashed square); (d) the ellipse template matched for the lumen contour; and (e) the detected (yellow solid line) and manually traced (cyan dashed line) lumen contours.

iteration time $k < [\alpha N]$, the hybrid PSO is used, and when $k \geq [\alpha N]$, the conventional PSO is used. Here, $[\cdot]$ is the operator of rounding, N is the total number of iterations, and $\alpha \in [0, 1]$ is a proportional coefficient.

To accelerate the searching with PSO, the parameters in (3) are limited to a certain range. First, for media-adventitia contour detection, we limit the distance between (x_c, y_c) and the center of ROI, to a number D_c, and r_a and r_b to a range from r_{min} to r_{max}. Then, for lumen contour detection, r_{max} is updated to half the major axis of the ellipse found in media-adventitia contour detection.

D. Contour Refinement

The contours detected by the ellipse template matching and PSO are close but still coarse estimation of the desired contours. They are subsequently refined by snake evolution. Here we use an adaption of snakes, called BVF snakes [10], which reduces computational requirement and improves capture range. We take advantage of BVF snakes to lead the initial contours to the refined contours. (For details, see [10].)

III. Experiments and Results

A. Image Acquisition and Parameter Setting

In vivo IVUS images were acquired at the Department of Cardiology, Zhongshan Hospital of Fudan University, Shanghai, China, by using an IVUS imaging system iLAB™ (Boston Scientific, USA) with a 310F 40-MHz Atlantis mechanical catheter (Boston Scientific, USA). In total, 88 IVUS images of coronary arteries were captured from 21 patients and digitized with 8-bit gray scale and resolution of 45 pixels/mm. Lumen and media-adventitia contours in all 88 images were manually traced by experienced physicians to serve as the ground truth.

The proposed method was validated on *in vivo* images with parameters empirically set as follows. The intensity outside the outer ellipse T_{bg} was set as 0.3 and -0.7 for detection of lumen and media-adventitia contours, respectively. In PSO, the particle number was 24, the iteration times of PSO were 150, the inertial function $\varphi(k) = 0.9 - 0.0045k$, acceleration constants α_1 and α_2 both equaled to 2, and the proportional coefficient α was set as 0.8. The parameters to limit searching range of PSO were given by: $D_c = 1.5$ mm, $r_{min} = 0.75$ mm, and $r_{max} = 3$ mm. The iteration times of BVF snakes were 60.

B. Qualitative Results

Results of contour initialization are depicted in Fig. 2. It was demonstrated that the proposed method yielded initial contours close to the manually traced contours. The new ROI for lumen contour extraction was smaller than the ROI for media-adventitia contour extraction, which was helpful for efficiently and effectively initializing the lumen contour.

Results of contour refinement are shown in Fig. 3. The proposed method was compared with manual tracing and the texture-RBF method [3]. The contours detected by the texture-RBF method (Fig. 3c and Fig. 3g) were disturbed and attracted by spurious edges resulting from speckle noise. In contrast, all contours detected by our method (Fig. 3b and Fig. 3f) were very close to the ground truth (Fig. 3d and Fig. 3h), demonstrating the accuracy and robustness of the algorithm.

C. Quantitative Results

To quantitatively evaluate the accuracy of the contour detection algorithms, automatically detected contours were compared with the ground truth. The accuracy was quantified with the following two standard measures, including the mean distance error (MD) and relative mean distance error (RMD). Suppose $\boldsymbol{p}$ is a discrete contour point detected by automated algorithms, and $\boldsymbol{q}$ is its closest point in the ground truth curve. The distance between $\boldsymbol{p}$ and $\boldsymbol{q}$ is denoted as $D(\boldsymbol{p})$. The relative distance is $RD(\boldsymbol{p}) = D(\boldsymbol{p})/d(\boldsymbol{q}, \boldsymbol{O})$, where $\boldsymbol{O}$ is the center of the ground truth curve, and $d(\boldsymbol{q}, \boldsymbol{O})$ is the distance between $\boldsymbol{q}$ and $\boldsymbol{O}$. Then MD and RMD are given by [1]:

$$\mathrm{MD} = \mathrm{mean}_p(D(\boldsymbol{p})), \tag{9}$$

$$\mathrm{RMD} = \mathrm{mean}_p(RD(\boldsymbol{p})) \times 100\%. \tag{10}$$

As enumerated in Table I, the proposed method yielded lower MD and RMD values compared to the texture-RBF method, suggesting the proposed method was superior to the texture-RBF method in terms of contour localization. The proposed method decreased MD (RMD) for lumen and media-adventitia contours by 3.1 pixels (2.7%) and 4.4 pixels (6.8%), respectively. The average improvement for two contours was 3.8 pixels and 4.8% in terms of MD and RMD, respectively.

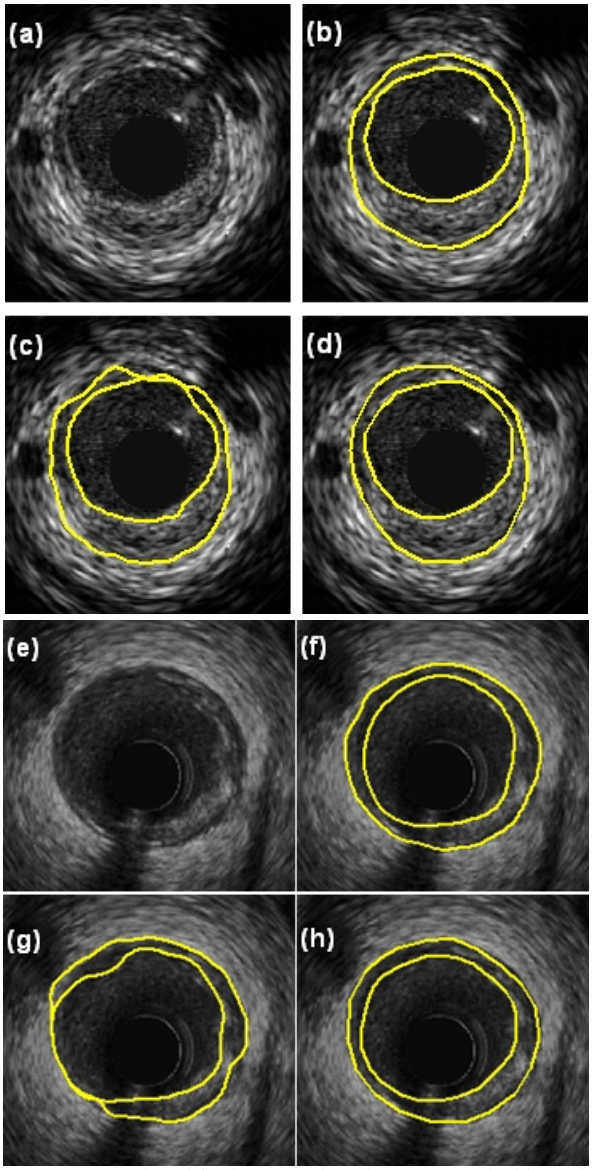

Fig. 3. Two examples of final contour detection, contrasted with results of the texture-RBF method. (a, e) IVUS images; (b, f) the results by the proposed method; (c, g) the results by the texture-RBF method; and (d, h) the ground truth.

TABLE I
QUANTITATIVE COMPARISON OF METHODS FOR CONTOUR DETECTION

Contours	Methods	MD (pixels)	RMD
Lumen contour	The proposed method	6.6±3.3	9.6%±4.8%
	Texture-RBF method	9.7±3.9	12.3%±5.5%
Media-adventitia contour	The proposed method	7.1±7.3	6.1%±5.7%
	Texture-RBF method	11.5±5.8	12.9%±6.2%

IV. DISCUSSION

The intensity outside the outer ellipse T_{bg} was set to 0.3 and -0.7 for detection of lumen and media-adventitia contours, respectively. In the experiments, we also examined the role of T_{bg} by varying its values from -1 to 1, with an interval of 0.1. When T_{bg} was between -0.8 and -0.5, the matching algorithm almost always found an ellipse close to the media-adventitia contour, and when T_{bg} was between 0.2 and 0.4, it almost always found an ellipse near the lumen contour. When T_{bg} was set to -1 or -0.9, the method tended to find a large ellipse containing a big part of adventitia, and when it was set larger than 0.4, the matched ellipse might shrink to the round catheter. When it was valued from -0.4 to 0.1, the method appeared ambiguous in finding the lumen or media-adventitia contours. It will be investigated in the future to determine an adaptive T_{bg} by analysis of the global and local intensities in IVUS images.

RMD values of lumen contour detection obtained by our method were larger than those of media-adventitia contour detection (Table I), suggesting the method might perform worse for lumen contours. We attributed it to the phenomenon that lumen contours appeared less elliptic and more irregularly shaped than media-adventitia contours.

V. CONCLUSION

In the paper, a method is proposed for detection of lumen and media-adventitia contours in IVUS images. It integrates ellipse template matching with PSO to initialize the contours and uses the BVF snakes to refine them. Results on 88 *in vivo* images demonstrated the performance of the method. The method will be incorporated into the characterization of atherosclerotic plaques in a future study.

REFERENCES

[1] D. Gil, A. Hernandez, O. Rodriguez, J. Mauri, and P. Radeva, "Statistical strategy for anisotropic adventitia modelling in IVUS," *IEEE Trans. Med. Imaging,* vol. 25, pp. 768-78, Jun 2006.

[2] M. H. Cardinal, J. Meunier, G. Soulez, R. L. Maurice, E. Therasse*, et al.*, "Intravascular ultrasound image segmentation: a three-dimensional fast-marching method based on gray level distributions," *IEEE Trans. Med. Imaging,* vol. 25, pp. 590-601, May 2006.

[3] M. Papadogiorgaki, V. Mezaris, Y. S. Chatzizisis, G. D. Giannoglou, and I. Kompatsiaris, "Image Analysis Techniques for Automated IVUS Contour Detection," *Ultrasound Med. Biol.,* vol. 34, pp. 1482-1498, 2008.

[4] R. Sanz-Requena, D. Moratal, D. R. García-Sánchez, V. Bodí, J. J. Rieta*, et al.*, "Automatic segmentation and 3D reconstruction of intravascular ultrasound images for a fast preliminar evaluation of vessel pathologies," *Comput. Med. Imag. Grap.,* vol. 31, pp. 71-80, 2007.

[5] W. Liu, J. A. Zagzebski, T. Varghese, C. R. Dyer, U. Techavipoo*, et al.*, "Segmentation of elastographic images using a coarse-to-fine active contour model," *Ultrasound Med. Biol.,* vol. 32, pp. 397-408, 2006.

[6] C. Di Mario, G. Gorge, R. Peters, P. Kearney, F. Pinto*, et al.*, "Clinical application and image interpretation in intracoronary ultrasound," *Eur. Heart J.,* vol. 19, pp. 207-29, Feb 1998.

[7] X. Zhang, C. R. McKay, and M. Sonka, "Tissue characterization in intravascular ultrasound images," *IEEE Trans. Med. Imaging,* vol. 17, pp. 889-899, Dec 1998.

[8] M. Lvbjerg, T. K. Rasmussen, and T. Krink, "Hybrid particles swarm optimizer with breeding and subpopulations," in *Proc. 3rd Genetic Evolutionary Computation Conf.*, San Francisco, CA, 2001, pp. 469-476.

[9] M. P. Wachowiak, R. Smolikova, Z. Yufeng, J. M. Zurada, and A. S. Elmaghraby, "An approach to multimodal biomedical image registration utilizing particle swarm optimization," *IEEE Trans. Evol. Comput.,* vol. 8, pp. 289-301, Jun 2004.

[10] K. W. Sum and P. Y. S. Cheung, "Boundary vector field for parametric active contours," *Pattern Recogn.,* vol. 40, pp. 1635-1645, 2007.